JOURNAL OF GEOPHYSICAL RESEARCH: ATMOSPHERES, VOL. 118, 1299–1311, doi:10.1002/jgrd.50156, 2013

A climatology of frozen-in anticyclones in the spring arctic stratosphere over the period 1960–2011

Rémi Thiéblemont,[1] Yvan J. Orsolini,[2] Alain Hauchecorne,[3] Marc-Antoine Drouin,[4] and Nathalie Huret[1]

Received 23 March 2012; revised 20 December 2012; accepted 27 December 2012; published 14 February 2013.

[1] During springtime, following the stratospheric final warming, intrusions from low latitudes can become trapped at polar latitudes in long-lived anticyclones. Such "frozen-in" anticyclones (FrIACs) have occasionally been observed to persist as late as August, advected by summer easterlies.

[2] In this study, the high-resolution advection contour model MIMOSA is used to advect a pseudo-potential vorticity tracer. The model is driven by ERA-40 and the ERA-Interim reanalyses over the period 1960–2011. We first identify a remarkable FrIAC event in spring 2011. In addition, we developed a method to detect the characteristic size of low-latitude intrusions into the polar region at the time of the spring transition, over the period 1960–2011. Years are classified as either Type-A when the intrusions are small or as Type-B when intrusions are large, potentially evolving into FrIACs. For a FrIAC to occur, we require an additional criterion based on the in-phase character of the core of the intrusions and the anticyclone.

[3] During the 52 analyzed years, 9 events have been identified: 1 in the 1960s, 1 in the 1980s, 2 in the 1990s, and 5 from 2002. FrIAC are predominantly long-lived intrusions, which occur in association with abrupt and early reversal to summer easterlies with a large heat flux pulse around the date of this wind reversal. Finally, the results are discussed in a climatological context.

Citation: Thiéblemont, R., Y. J. Orsolini, A. Hauchecorne, M.-A. Drouin, and N. Huret (2013), A climatology of frozen-in anticyclones in the spring arctic stratosphere over the period 1960–2011, *J. Geophys. Res. Atmos.*, *118*, 1299–1311, doi:10.1002/jgrd.50156.

1. Introduction

[4] The onset of the stratospheric final warming (hereinafter SFW) marks the winter-to-summer transition in the Arctic stratosphere, when the summer easterly circulation begins to develop. During this transition, the polar vortex breaks up into "remnants" which can persist as coherent vortices for several months [*Hess*, 1991] due to the weak horizontal and vertical wind shears. *Orsolini* [2001] found evidence of "fossil" debris from the polar vortex persisting until August in three-dimensional transport simulations of the long-lived nitrous oxide (N_2O) tracer. *Durry and Hauchecorne* [2005] detected the presence of long-lived vortex remnants in the midlatitude summer stratosphere between 20 and 25 km, using balloon-borne observations of several trace species by a diode laser spectrometer, hence confirming these results.

[5] Recent studies have shown that, following the spring onset, low-latitude air could similarly be transported to high latitudes and remain confined, persisting for a long time within a stable anticylone embedded in the summer easterlies. Using water vapor (H_2O) and N_2O measurements from the Microwave Limb Sounder (MLS) aboard the AURA satellite, *Manney et al*. [2006] reported for the first time such a long-lived "frozen-in" anticyclone (FrIAC) in the polar stratosphere during 2005 spring and summer. This FrIAC event started as a low-latitude intrusion which was quickly advected poleward during an abrupt and strong SFW. This intrusion then developed into an anticyclone extending in the vertical range 650–1400 K, advected by high-latitude easterlies and persisting until late August 2005. Based on examination of analyzed potential vorticity (PV) maps, they suggested that other cases occurred in 1982, 1994, 2003, and possibly in 1997 and 2002. Subsequently, other FrIACs have been confirmed in spring 2003 in MIPAS (Michelson Interferometer for Passive Atmospheric Sounding) observations [*Lahoz et al*., 2007] and again in MLS observations in spring 2007 [*Thiéblemont et al*., 2011].

[6] Several model studies have focused on the occurrence of FrIACs. *Allen et al*. [2011] further modelled the evolution

All supporting information may be found in the online version of this article.

[1]LPC2E–Laboratoire de Physique et Chimie de l'Environnement et de l'Espace/CNRS, Université d'Orléans, Orléans, France.
[2]NILU–Norwegian Institute for Air Research, Kjeller, Norway.
[3]LATMOS–Laboratoire Atmosphères, Milieux, Observations Spatiales/CNRS, Quartier des Garennes, Guyancourt, France.
[4]OMP–Observatoire Midi-Pyrénnées/CNRS, Toulouse, France.

Corresponding author: R. Thiéblemont, LPC2E–Laboratoire de Physique et Chimie de l'Environnement et de l'Espace/CNRS, Université d'Orléans, 3A, Avenue de la Recherche scientifique, F-45071, France. (remi.thieblemont@cnrs-orleans.fr)

2169-897X/13/10.1002/jgrd.50156

and decay of the 2005 FrIAC using 2D and 3D models of varying complexity. *Thiéblemont et al*. [2011] also used the PV contour advection model MIMOSA (Modélisation Isentrope du transport Méso-échelle de l'Ozone Stratosphérique par Advection) [*Hauchecorne et al*., 2002] over the last decade (2000–2009) to show that FrIACs are favored if (i) no deep sudden stratospheric warming occurs during winter and if (ii) the Quasi-Biennal Oscillation (QBO) is in easterly phase. Recently, *Allen et al*. [2012] performed a climatology of tracer transport during SFW using the tracer equivalent latitude (hereinafter TrEL) diagnostic over a 33-year period (1979–2011). By examining the decrease of TrEL averaged northward of 80°N from 10 May to 20 June, they found evidences of FrIACs in 1982, 1994, 1997, 2000, 2002, 2003, 2004, 2005, and 2011.

[7] Occurrences of FrIAC events are closely linked to planetary wave activity, sudden stratospheric warmings (SSWs) and SFWs [*Manney et al*., 2006; *Thiéblemont et al*., 2011]. Albeit our knowledge of SSWs and SFWs has greatly advanced over the last few decades [*Black et al*., 2006; *Black and McDaniels*, 2007; *Charlton and Polvani*, 2007; *Matthewman et al*., 2009; *Ayarzagüena and Serrano*, 2009; *Waugh and Polvani*, 2010], the origin of the planetary wave variability in the stratosphere is not always known, and *Nishii et al*. [2011], for example, recently showed that tropospheric blockings can either lead to a strong or weak stratospheric vortex, depending on their longitudinal location.

[8] In this paper, we systematically investigate the characteristics of FrIACs (i.e., frequency of occurrence, spatial extent and origin of low-latitude air masses) in a climatological context from 1960 to 2011. The study is based on advected PV by the contour advection model MIMOSA [*Hauchecorne et al*., 2002] and on wind, temperature, pressure, and geopotential height fields from ERA-40 and ERA-Interim reanalyses. Section 2 described the modeling tools used. In section 3, we investigate the 2011 spring, during which a remarkable FrIAC event occurred. The stratospheric dynamical conditions related to this FrIAC are compared with those found in *Thiéblemont et al*. [2011]. This new event motivated us to establish a detailed climatology of FrIACs that we describe in the forthcoming sections. In section 4, we carry out a systematic study over the 1960–2011 period of low-latitude intrusions to the polar region during the winter-to-summer transition. Such intrusions can occasionally lead to the development of a FrIAC. The occurrences and characteristics of FrIACs are further examined in section 5. Sections 6 and 7 are devoted to discussion and concluding remarks.

2. MIMOSA Model

[9] Potential vorticity fields have been calculated using the MIMOSA contour advection model [*Hauchecorne et al*., 2002]. This model performs high-resolution, isentropic advection of PV based on the analyzed wind, pressure, and temperature fields. PV is initially computed at a resolution of 1.125° in latitude and longitude (T106), and vertically interpolated on an isentropic surface. This field is then interpolated on the model x-y grid centered on the North Pole with a horizontal resolution of 37 × 37 km (three grid points/degree) and advected with a time step of 1 hour.

[10] To preserve the homogeneity of the field, a regridding of the PV field on the original grid is made every 6 hours. This regridding lead to numerical diffusion which is minimized by using an interpolation scheme based on the preservation of the second-order momentum of the PV perturbation. Diabatic changes in the PV field at large scales are accounted by applying a relaxation toward the European Centre for Medium-Range Forecast (ECMWF) ERA-Interim (or ERA-40) PV field with a time scale of 10 days. To preserve the filamentation structure, the relaxation term is only applied to scales larger than 300 km. This technique allows MIMOSA to run continuously over periods of several months and to follow the evolution of dynamical barriers and fine-scale structures such as vortex remnants and tropical intrusions [*Godin et al*., 2002; *Marchand et al*., 2003; *Leblanc et al*., 2004 and *Huret et al*., 2006]. Hence, the quantity advected by the model is not the true dynamical PV but a "quasi-passive PV," which correlates well with the long-lived trace species in the stratosphere [*Hauchecorne et al*., 2002].

[11] The MIMOSA simulations are initialized and forced using the meteorological fields of the ERA-40 reanalyses [*Uppala et al*., 2005] from 1960 to 1979. We then use ERA-Interim reanalyses [*Dee et al*., 2011] from 1980 to the present. ERA-40 reanalyses are distributed on 23 pressure levels, while ERA-Interim are distributed on 37 pressure levels from 1000 to 1 hPa, with a vertical resolution of 3 km approximately in the stratosphere. Those covering the middle stratosphere are the same in both reanalyses. Comparisons between ERA-40 and ERA-Interim reanalyses have revealed that the stratospheric circulation has been considerably improved in ERA-Interim, essentially due to the use of a 4-D variational assimilation scheme (instead of 3-D), a correction of biases in satellite radiance observations, and a much higher horizontal resolution model [*Dee et al*., 2011]. This motivates our use of ERA-Interim in the overlapping period.

[12] To investigate the dynamical conditions associated with FrIACs and with low-latitude intrusions occurring in the winter and spring Arctic stratosphere, 6-month runs starting from the first of January were performed for every year for the period 1960–2011. The series of 52 runs has been made on the 850 K (~31 km, ~10 hPa) isentropic surface. To investigate in more detail, the vertical evolution of the FrIAC in 2011, we performed 61 additional runs, which have been initiated from 1 March and continued until 30 June, between 350 K and 950 K isentropic levels, and with a regular vertical step of 10 K. Zonal and meridional winds, as well as temperature fields from the ERA-40 and ERA-Interim reanalyses have also been used to establish a climatology of the Northern Hemisphere zonal-mean zonal winds and meridional heat fluxes over the last decade.

3. Spring 2011: Dynamical Investigations

[13] Figure 1a shows the evolution of the zonally averaged zonal wind over the Northern Hemisphere from 1 January to 1 June 2011 at 10 hPa, approximately corresponding to the 30 km altitude. As a diagnostic of the wave activity in the middle stratosphere [*Andrews et al*., 1987], Figure 1b shows the evolution of the zonal-mean meridional eddy heat flux ($<v'T'>$ expressed in $K \cdot m \cdot s^{-1}$) at 30 hPa and averaged in

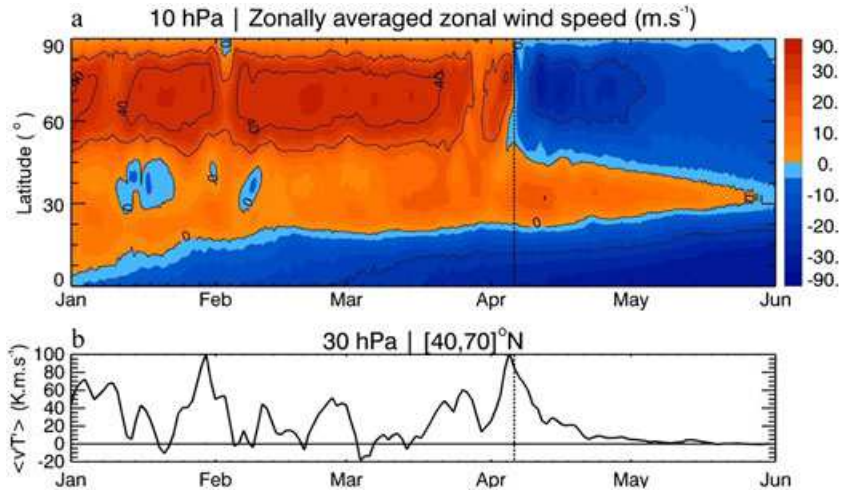

Figure 1. (a) Time series of the ERA-Interim zonal-mean zonal wind (in m/s) from 1 January to 1 June 2011 at 10 hPa over the Northern Hemisphere (b) zonal-mean meridional eddy heat flux averaged over the [40,70]°N latitude range at 30 hPa. The vertical dashed lines correspond to the turnover date of April 6.

the [40,70]°N latitude range. At high latitudes, a strong westerly circulation associated with the Arctic polar vortex prevails in early winter. By late January, a weakening of the polar vortex coincides with a strong enhancement of the meridional eddy heat flux. While the strongest wave events can lead to a SSW, a zonal wind reversal at 60°N did not occur in this case. Note that a major SSW is defined as the reversal of the westerlies at 10 hPa and 60°N [*WMO*, 2007]. The wave activity remained unusually weak during the rest of the winter [*Hurwitz et al*., 2011], allowing the westerlies to recover and leading to an extraordinary strong and persisting cold polar vortex in February and March, well centered above the North Pole [*Manney et al*., 2011]. In late March, the heat flux anomaly sharply increased, reaching values close to $100\,K \cdot m \cdot s^{-1}$ by early April. This wave activity enhancement contributed to decelerate and reverse the polar westerlies (Figure 1a). Such conditions of abrupt reversal are similar to those occurring during the 2005 SFW [*Manney et al*., 2006]. In addition, at tropical latitudes, the QBO was well established in an easterly phase, leading to a strong anticyclonic zonal wind shear between the tropical and midlatitudes. In these favorable dynamical conditions, i.e., absence of a midwinter major SSW and a QBO in easterly phase [*Thiéblemont et al*., 2011], a FrIAC occurred during the SFW in early April.

[14] Figure 2 displays the three-dimensional evolution of the polar vortex and of low-latitude intrusions from the end of March to April, from 350 to 950 K. In these plots, polar or low-latitudes air masses correspond to the Lait-PV [*Lait*, 1994] normalized at 380 K higher than 11 or lower than 5.5 PV units ($1\ PVU = 10^{-6}.m^2.s^{-1}.K.kg^{-1}$), respectively. These values correspond roughly to 400/200 PVU at 850 K, respectively.

[15] On 30 March, the polar vortex (Figure 2a in blue) is still well formed from 350 to 950 K and begins to be displaced southward along the Greenwich meridian. Thin, elongated filaments eroded from the vortex by wave breaking are seen above North America at the higher levels. Five days later (Figure 2b), the polar vortex is distorted while a large low-latitude intrusion occurs above East Asia in the [650,950] K vertical range (in red). The low-latitude air mass in the anticyclone above the North America results from a previous, thinner intrusion which has been pushed away from polar latitudes by the above-mentioned intrusion above East Asia. Below 650 K, a more strongly distorted polar vortex prevails along with several low-latitude intrusions.

[16] From April 4 to 9, the large-scale intrusion identified previously further develops into an anticyclone which remains located above North-East Asia/North-West America, near the longitude of the climatological Aleutian High [*Harvey and Hitchman*, 1996; *Harvey et al*., 2002] (See animations in the supporting information which corresponds to the vortex, vortex/FrIAC, and FrIAC evolution (Figures 2a, 2b, and 2c), respectively). At the same time, the polar vortex further sheds filaments. By April 10, the polar vortex irreversibly breaks up while the anticyclone is advected above the North Pole[1]. On 20 April (Figure 2c, in red), the anticyclone is well located above the North Pole, trapped into the polar anticyclonic circulation and persisting until late May (see the supporting information). The thin tongue in the vicinity of what has become the FrIAC anticylone, opposite to the pole, results from an intrusion originating around 18 April, at the time of the last peak in the meridional heat flux (Figure 1b).

[17] To compare the characteristics of the 2011 FrIAC event to those of previous events (i.e., spatial extent and origin of low-latitude air masses), we perform in the next two sections a FrIAC climatology over the 1960 to 2011 period.

4. Detection of Low-Latitude Air Masses in the Polar Region

[18] To identify the low-latitude intrusions pulled toward polar latitudes and to estimate their spatial extent, we established a systematic method based on the concept of equivalent latitude [*Allen and Nakamura*, 2003] and applied it to the PV advected by the MIMOSA model. Since the previous studies of FrIAC events in 2003, 2005 [*Manney et al*., 2006; *Allen et al*., 2011], 2007 [*Thiéblemont et al*.,

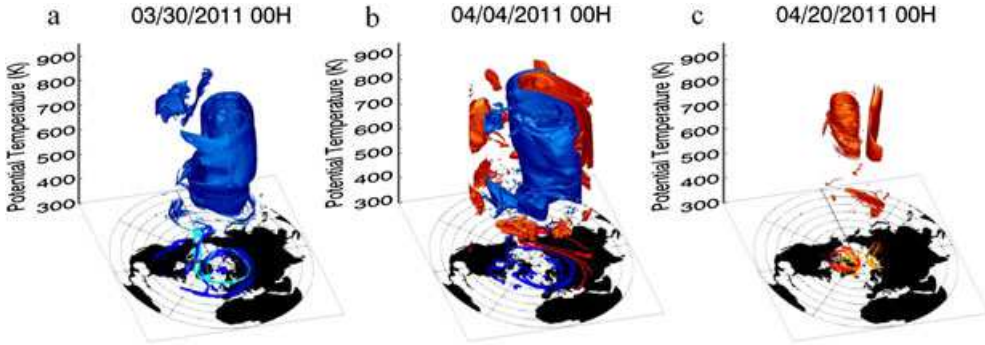

Figure 2. 3D representation of the evolution of the polar vortex and of low-latitude air masses versus potential temperature (in K) in spring 2011 on (a) March 30 (b) April 4 and (c) April 20. The blue/red colors correspond to a Lait-PV of 11 PVU/5.5 PVU, displaying the polar vortex and low-latitude air, respectively. The blue surface on panel (c) has been removed for clarity. The dark/light blue contour on the projected map depicts the 11 PVU at 950 K/450 K, respectively. The red/orange contour on the projected map depicts the 5.5 PVU at 950 K/650 K, respectively.

2011], and 2011 (this study) have shown that they occur as the high-latitude westerlies turn irreversibly to the summer easterlies, we begin by defining more precisely this "turnover" date. In the rest of this paper, it is defined as the day when the zonal-mean zonal wind at 10 hPa and 60°N becomes irreversibly easterly, and it will be referred to as the "day 0." Figure 3 reveals that this turnover date displays a high degree of interannual variability over the period 1960–2011 and in particular during the 1980s and 2000s. However, between 1991 and 1996, the turnover dates are always included between 5 and 15 April. Such a low interannual variability in the mid-90s was also observed in the vortex breakup dates [*Waugh and Rong*, 2002].

[19] The relation between the distribution of a given tracer isoline q and the equivalent latitude is given by [*Allen and Nakamura*, 2003]

$$\Phi_{eq,q} = \sin^{-1}\left(\frac{A_q}{2\pi a^2} - 1\right) \quad (1)$$

where A_q (in m^2) corresponds to the surface enclosed by a given tracer isoline (here the advected PV) at a time t and an isentropic surface θ, a represents the earth radius (in m).

[20] This relation allows obtaining the PV distribution as a function of the equivalent latitude Φ_{eq} over the whole Northern Hemisphere. We first calculate a PV threshold (hereinafter PV_{lim}) corresponding to a threshold of equivalent latitude (hereinafter $\Phi_{eq,lim}$) marking the upper limit of the intrusion latitudinal origin (e.g. originating from latitude equatorward of 40°N or 30°N, for example). This relation is established when the equivalent latitude is initially calculated. The next step consists in calculating the spatial extent of these low-latitude air parcels northward of a given latitude circle, hereinafter Φ_{circle}. At each time step, we calculate the distribution of the PV equivalent latitude between the pole and the Φ_{circle}. Thus, using the PV_{lim} threshold, we can define the $\Phi'_{eq,lim}$ associated to the new distribution of equivalent latitude northward of the Φ_{circle}. Finally the spatial extent within the latitude circle (hereinafter S_{lim}) of the air parcels characterized by PV lower or equal to PV_{lim} is

$$S_{\lim} = 2\pi a^2\left(\sin\left(\Phi'_{eq,\lim}\right) - \sin(\Phi_{circle})\right) \quad (2)$$

S_{lim} is expressed in m^2. If the term $2\pi a^2$ is omitted and the result multiplied by 100, S_{lim} is expressed in percentage of the Northern Hemisphere area (hereinafter %NH). The latitude Φ_{circle} circumscribing the polar region is here chosen as 60°N. The tracer that we use is the MIMOSA-advected PV (hence is not the true dynamical PV), and it does not allow following a FrIAC until summer because of the applied diabatic relaxation. Due to these processes, we lose the PV signature of a FrIAC more quickly than if using a long-lived chemical tracer [*Manney et al.*, 2006; *Allen et al.*, 2011] or a TrEL [*Allen and Nakamura*, 2003; *Allen et al.*, 2012]. Nevertheless, it allows following intrusions and their potential development into FrIACs, as shown for the 2007 case by *Thiéblemont et al.* [2011] and for the 2011 case in section 3.

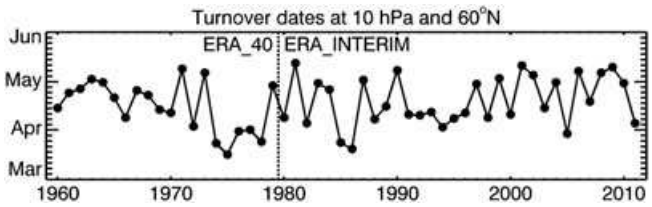

Figure 3. Turnover dates of the Northern Hemisphere calculated over the 1960–2011 period at 10 hPa and 60°N using ERA-Interim and ERA40.

4.1. Sensitivity Tests

[21] Tests have been performed to evaluate the method sensitivity to the choice of the equivalent latitude threshold $\Phi_{eq,lim}$ (i.e., 50°N, 40°N or 30°N, for example) and are illustrated here for the 2011 FrIAC case, when the turnover occurred on 5 April. Maps of advected PV lower or equal to the PV_{lim} are represented 20 days after the turnover date on Figure 4a, for the three equivalent latitude thresholds $\Phi_{eq,lim}$ mentioned above. At that time, the FrIAC is strongly established over the North Pole. Clearly, the choice of the $\Phi_{eq,lim}$ strongly influences the spatial extent of the air masses trapped in the FrIAC. Moreover, the PV field is not constant

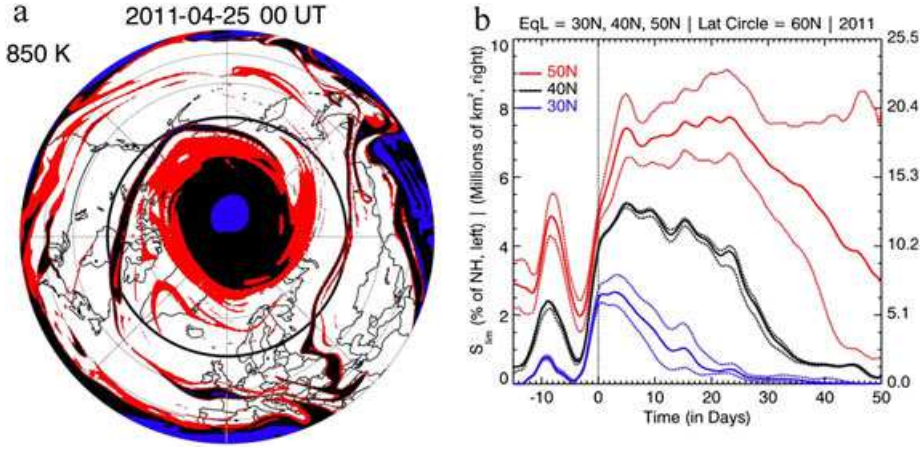

Figure 4. (a) MIMOSA PV fields with values lower than PV_{lim} for $\Phi_{eq,lim} = 30°N$, 40°N and 50°N (in blue, black and red, respectively) on 25 April 2011 at 850 K. (b) Time evolution of the spatial extent S_{lim} northward of 60°N obtained for $\Phi_{eq,lim} = 30°N$, 40°N and 50°N, respectively, at 850 K. Spatial extent is expressed either in %NH (left axis) and in millions squared kilometers (right axis). In Figure 4b, the vertical dashed (solid) line denotes the turnover date (see text).

during the evolution of the simulation, and PV varies around the turnover period in particular. We use the interval ΔPV_{lim} of these (small) variations to define a "confidence interval" ΔS_{lim} on the spatial extent S_{lim}.

[22] Figure 4b shows the evolution of S_{lim} for the three equivalent latitude thresholds along with the confidence interval ΔS_{lim}. At the onset of the turnover (vertical dashed line), a rapid enhancement of the intrusion spatial extent is observed for $\Phi_{eq,lim} = 30°N$, 40°N, and 50°N, increasing from 0%NH to 2.5%NH, from 0.5%NH to 5.0%NH, and from 2.0%NH to 7.5%NH, respectively. This enhancement characterizes the development and poleward extension of the intrusion associated to the FrIAC. Subsequent brief enhancements (for example, on the day 16) are due to thin intrusions penetrating into the polar region. The confidence interval ΔS_{lim} is depicted by the difference between the dashed curves. The ΔS_{lim} is the smallest for the $\Phi_{eq,lim} = 40°N$, close to 0.3%NH, while it is the largest for $\Phi_{eq,lim} = 50°N$. Furthermore, in the latter case, ΔS_{lim} is seen to increase with time. While we have illustrated the sensitivity of the method for the 2011 FrIAC case, we have further tested $\Phi_{eq,lim}$ and ΔS_{lim} for the whole period covered 1960–2011 (not shown for brevity). For the rest of this paper, we use $\Phi_{eq,lim} = 40°N$ and $\Delta S_{lim} = 0.3\%NH$, which corresponds to the climatological confidence interval obtained.

4.2. Low-Latitude Intrusions Over 1960–2011

[23] Given the results above, we apply the method for each year between 1960 and 2011 using $\Phi_{eq,lim} = 40°N$. The spatial extents S_{lim} (in %NH) are grouped in decades in Figure 5. Regardless of the year considered, the period before the turnover is characterized by a strong variability of the S_{lim}, as low-latitude intrusions are pulled out northward of 60°N but do not remain at polar latitudes, being either quickly distorted or displaced southward due to wave activity. After the turnover, S_{lim} depicts smoother oscillations and finally decreases slowly in the easterly summer regime.

[24] From examination of Figure 5, it appears that years can be classified in two types. For Type-A years (gray-colored curves), S_{lim} is lower than the 0.3%NH threshold (horizontal dashed line) at day 0. Several Type-A years have been identified in each decade: three in the 1960s, three in the 1970s, five in the 1980s, three in the 1990s, four in the 2000s, and one in the current decade, i.e., 19 in total. Since no low-latitude air masses are then detected after the turnover, these years are not considered as favorable for the formation of a FrIAC.

[25] In Type-B years, low-latitude intrusions are higher than the threshold 0.3%NH after the turnover. Again, several Type-B years have been identified in each decade: 7 in the 1960s, 7 in the 1970s, 5 in the 1980s, 7 in the 1990s, 6 in the 2000s, and 1 in the current decade, i.e., 33 in total. In Type-B years, the duration over which S_{lim} remains above the detection threshold displays a high degree of interannual variability, from 3 days in 2004 until over 45 days in 1982, 2005, 2007, and 2011. The long persistence of the intrusions, for example, largely exceeding 20 days in 1966 (Figure 5a), 1978 (Figure 5b), 1982 or 1986 (Figure 5c), 1994 (Figure 5d), 2003, 2005, 2007, or 2011 (Figures 5e and 5f), is a first indication of FrIAC occurrences. Thus, it would appear that besides the 4 FrIACs observed in satellite data in the 2000s (as mentioned in section 1), five additional FrIACs could have occurred in 1966, 1978, 1982, 1986, and 1994. However, additional diagnostics are needed to confirm this statement: FrIACs correspond to long-lived coherent anticyclones which indeed need to be identified. In the next section, we further investigate the Type-B years and establish a FrIAC climatology by examining the ERA-40 and ERA-Interim geopotential height fields associated with the low-latitude intrusions.

5. FrIACs Climatology

5.1. Occurrences

[26] In their paper, *Allen et al.* [2011] showed that, for several weeks after the intrusion, during what they termed the "anticyclonic phase," the FrIAC tracer anomaly (high N_2O in their case) is associated with a long-lived coherent anticyclone with the same shear as the background wind. By comparing the evolution of the vertical structure of

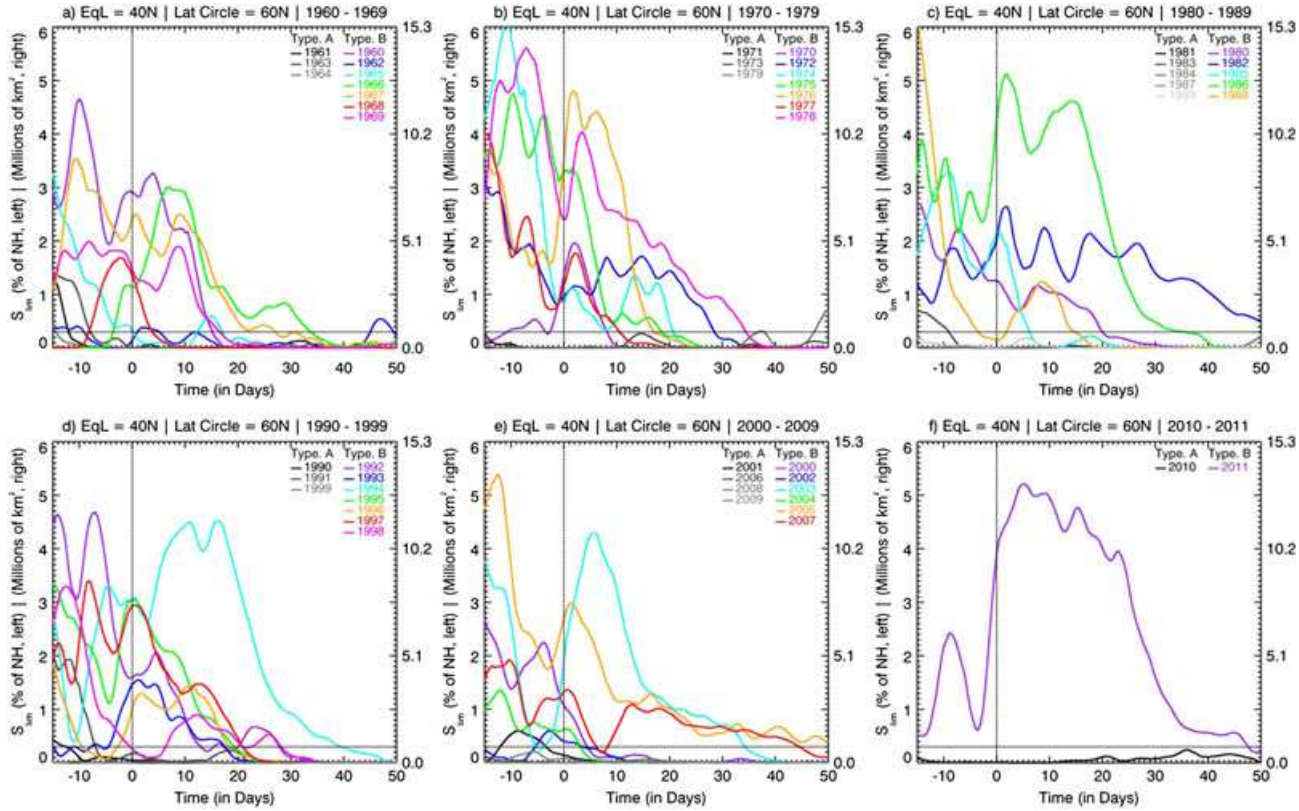

Figure 5. Time evolution of the spatial extent S_{lim} during the (a) 1960s, (b) 1970s, (c) 1980s, (d) 1990s, (e) 2000s, and (f) 2010s, computed northward of 60°N and for $\Phi_{eq,lim} = 40°N$. The horizontal dashed line at 0.3%NHA denotes the climatological confidence interval. Type-A years are shown in black or gray, while Type-B years are shown in color.

FrIACs in 2005 and 2007, *Thiéblemont et al*. [2011] showed that the onset of the shearing phase, when the FrIAC starts to stretch and mix with the background air, is similar in both cases occurring around mid-May. This transition coincides with the decay of the anticyclonic eddy due to diabatic processes [*Allen et al*., 2011], which merges with the large summer anticyclone. Thus, to confirm that the low-latitude intrusions described in the previous section led to FrIAC occurrences, we examine if they coexisted with a long-lived anticylonic eddy. This is done by calculating the distance (hereinafter $L_{GPH\text{-}PV}$) between the core of the intrusion (i.e., the lowest advected-PV values) and the core of the anticyclone (i.e., the maximum eddy geopotential height). The $L_{GPH\text{-}PV}$ is calculated northward of 70°N, where the core of FrIACs in 2003, 2005, and 2007 has been observed in previous studies. We expect to find a high correlation between these two quantities at least until the beginning of the shearing phase that we define on May 15, following the arguments of *Allen et al*. [2011] and *Thiéblemont et al*. [2011].

[27] Figure 6 shows the $L_{GPH\text{-}PV}$ in 1966, 1982, 1994, 1997, 2002, 2003, 2005, 2007, and 2011. The first vertical dashed line corresponds to the turnover day. The horizontal dashed line marks $L_{GPH\text{-}PV}$ equal to 1000 km, the distance which approximately separates the 100 m contours of eddy geopotential height as revealed in Figure 7. When $L_{GPH\text{-}PV}$ is lower than 1000 km, the PV minimum and geopotential height eddy are assumed to be "in-phase."

[28] On each panel, a sharp decrease of $L_{GPH\text{-}PV}$ below 1000 km is indeed observed following the turnover on 1 May 1966, 26 April 1982, 23 April 1994, 8 May 1997, 7 May 2002, 22 April 2003, 31 March 2005, 2 May 2007, and 4 April 2011. Such decreases indicate that the anticyclonic anomaly and the low-latitude intrusion are getting in-phase. Figure 7 shows maps of advected PV and geopotential height on these dates. On each map, the low PV (with equivalent latitude below $\Phi_{eq,lim} = 40°N$) is trapped inside the anticyclone core (red contours).

[29] Figure 6 reveals that, following the sharp decrease, $L_{GPH\text{-}PV}$ values remain low during several weeks, before gradually increasing in mid-May when the shearing phase starts (i.e., when the large summer anticyclone forms). This sharp decrease followed by a gradual increase hence forms a "bowl-shaped" structure which characterizes the anticyclonic phase. These periods are indicated by the gray background on each panel. The 1982, 2005, and 2011 FrIACs display the largest of such "bowls," which last 1.5, 2, and 2 months, respectively. The 1994, 2002, 2003, and 2007 "bowls" last between 3 weeks and 1 month. The 1966 and 1997 "bowls" are the shortest, with durations not exceeding 2 weeks. As mentioned above, we consider that a FrIAC occurs if $L_{GPH\text{-}PV}$ remains lower than 1000 km until the beginning of shearing phase which we define as May 15 of each year. After examining the Type-B years, we found 9 FrIAC events in 1966, 1982, 1994, 1997, 2002, 2003, 2005, 2007, and 2011 when using this second criterion.

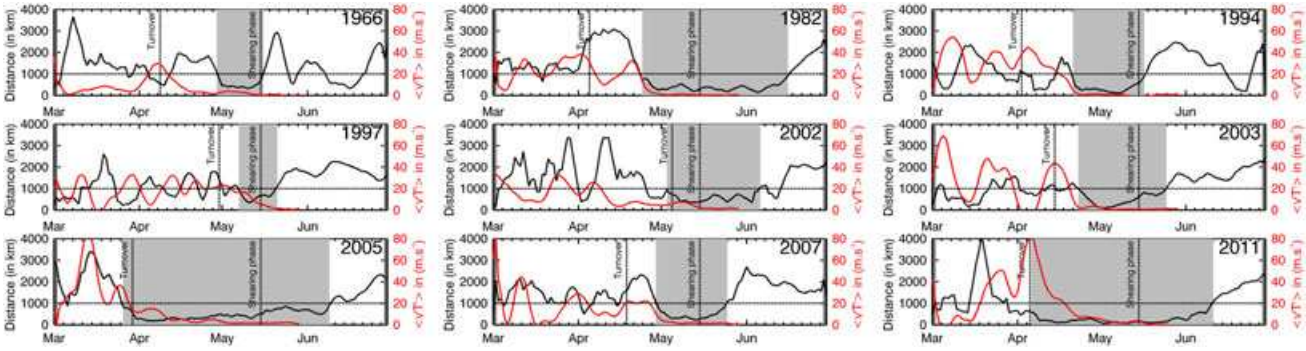

Figure 6. Distance $L_{GPH\text{-}PV}$ (in km) between the geopotential height maximum and the PV minimum northward of 70°N (black curve) at 850 K from 1 March to 30 June for the years 1966, 1982, 1994, 1997, 2002, 2003, 2005, 2007, and 2011. Also shown is the zonal-mean meridional eddy heat flux (red curve, in $K \cdot m \cdot s^{-1}$) averaged over the [40,70]°N latitude range at 30 hPa. The two vertical dashed lines denote the turnover dates and the mean onset of the shearing phase (May 15). The area in gray corresponds to the "bowl" period (see text).

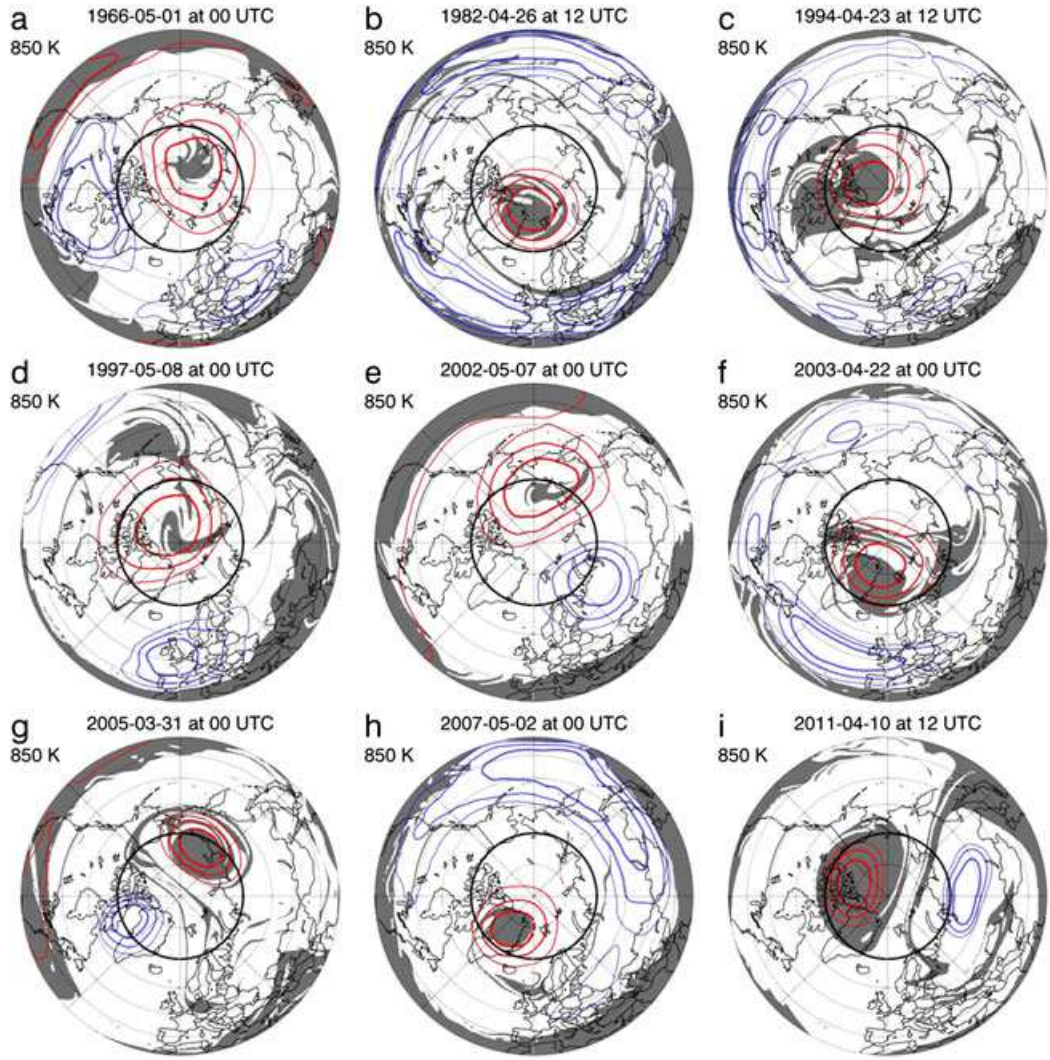

Figure 7. MIMOSA PV fields (gray-filled contours) with values lower than PV_{lim} for $\Phi_{eq,lim} = 40°N$ on (a) 1 May 1966 00 UTC, (b) 26 April 1982 12 UTC, (c) 23 April 1994 12 UTC, (d) 8 May 1997 00 UTC, (e) 7 May 2002 00 UTC, (f) 22 April 2003 00 UTC, (g) 31 March 2005 00 UTC, (h) 2 May 2007 00 UTC, and (i) 4 April 2011 12 UTC. Also shown are isocontours of geopotential height anomalies; red (blue) curves indicate the departure of -100, -200, and -300 m (+50, +100, and +150 m) from the maximum (minimum) eddy geopotential height over the Northern Hemisphere.

[30] The 1994 $L_{GPH\text{-}PV}$ evolution shows a particular behavior since two bowls form, separated by a period when $L_{GPH\text{-}PV}$ reaches 1800 km: the first starting in late March and the second in late April. This indicates that two successive low-latitude intrusions occurred, over the North East America and then over the Arctic Ocean, as illustrated by the map of 23 April 1994 (Figure 7c). On this date, the first intrusion is no longer trapped into an anticyclone and starts to be sheared and stretched. Consequently, only the second intrusion defines a FrIAC.

[31] The zonal-mean meridional eddy heat fluxes averaged over the latitude band [40,70]°N are also shown in Figure 6, to follow the wave activity during the FrIAC evolution. Sharp pulses of eddy heat flux associated to the rapid displacement of warm, low-latitude air to the polar region are seen before the formation of the bowls in 1982, 1994, 1997, 2003, 2005, 2007, and 2011, peaking at maximum values of 38, 40, 40, 80, 20, and 80 $K \cdot m \cdot s^{-1}$, respectively. When the bowl starts, the eddy heat flux slightly decreases, as expected, following the establishment of the summer easterlies in polar region. Among the years with FrIAC occurrences, 1966 and 2002 are characterized by the lowest heat fluxes and also by a small spatial extent (Figures 7a and 7e).

[32] From the 33 Type-B years, we only consider that FrIACs occurred in nine cases, as most of the Type-B years do not reveal a bowl-shaped structure persisting after 15 May (using the 1000 km $L_{GPH\text{-}PV}$ threshold). Note that if the shearing phase onset was chosen 10 days earlier, only one more FrIAC would have been included (1998). In the next section, we investigate in detail the Type-B year 1986, which reveals one of the strongest low-latitude intrusion after the turnover (Figure 5c) but yet did not lead to a FrIAC, according to our criterion.

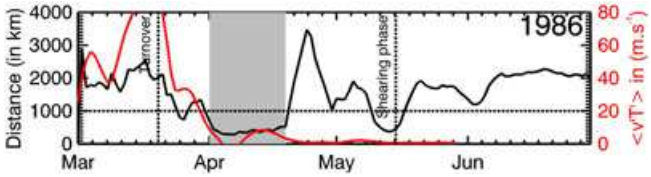

Figure 8. As for Figure 6 but for 1986.

5.2. A Case Study: 1986

[33] Figure 8 shows the $L_{GPH\text{-}PV}$ evolution and the associated eddy heat flux for 1986. As for other events (Figure 6), a strong pulse of eddy heat flux reaching 100 $K \cdot m \cdot s^{-1}$ is detected at the turnover day (around the 20 March). This wave activity enhancement is followed by the establishment of a bowl in early April. However, a second pulse of heat flux, albeit weak (not higher than 10 $K \cdot m \cdot s^{-1}$) occurred in mid-April. Shortly after, the $L_{GPH\text{-}PV}$ increases sharply, indicating the end of the bowl structure, around 1 month before the onset of the shearing phase.

[34] The evolution of PV and geopotential height is shown as a series of maps for three dates in Figure 9. When the bowl is formed by 12 April, the low-PV anomaly and the geopotential height are in phase (Figure 9a). On 20 April (Figure 9b), a second low-PV intrusion crosses the 60°N latitude circle above Eastern Europe following a heat flux pulse, hence contributing to destroy the phasing. On 26 April (Figure 9c), the low-PV lobe is no more trapped in the anticyclonic eddy and is quickly advected to midlatitudes and distorted by the wind shear. We do not identify such a case as a FrIAC since its signature is removed from the polar region before the beginning of the shearing phase. The absence of FrIACs during the mid-90s could be explained by a wave activity characterized by several such consecutive pulses, and we will return to this point in the Discussion section.

5.3. Characterization of the Latitudinal Origin of Air Masses in the Intrusion

[35] We next calculate the latitudinal origin of air masses with the low-PV intrusions associated to the nine FrIACs identified. Since the PV rapidly relaxes due to diabatic processes, we estimate the latitudinal origin at the beginning of the bowl formation. Thus, the PV_{lim} threshold is initialized by calculating the PV_{lim} averaged between -15 and 0 days before this new reference day. The spatial extents have been calculated northward of the $\Phi_{circle} = 60°N$ except in 1994 when the $\Phi_{circle} = 70°N$ has been chosen to remove a second lobe over the North East America, which is not associated with the FrIAC as shown previously (see section 5.1).

[36] Figure 10 presents the probability distribution functions (hereinafter PDFs) of latitudinal origin, expressed in

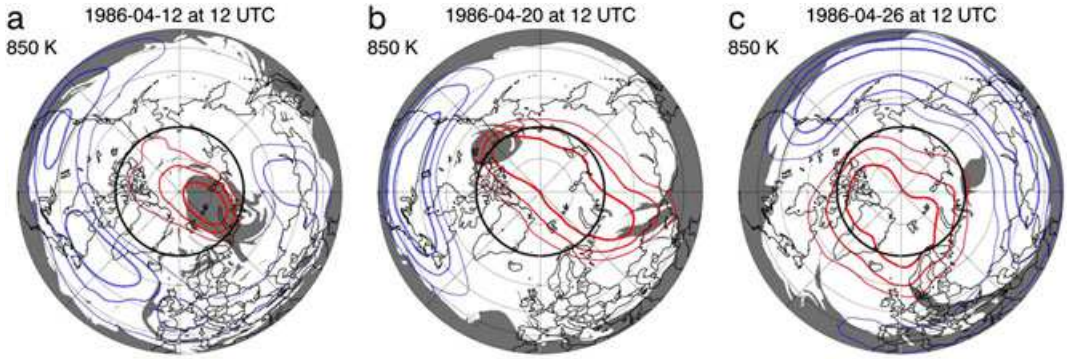

Figure 9. MIMOSA PV fields (gray-filled contours) lower than PV_{lim} calculated for $\Phi_{eq,lim} = 40°N$ in 1986, on (a) 12 April at 12 UTC, (b) 20 April at 12 UTC, and (c) 26 April at 12 UTC. Geopotential height anomalies are represented as for Figure 7.

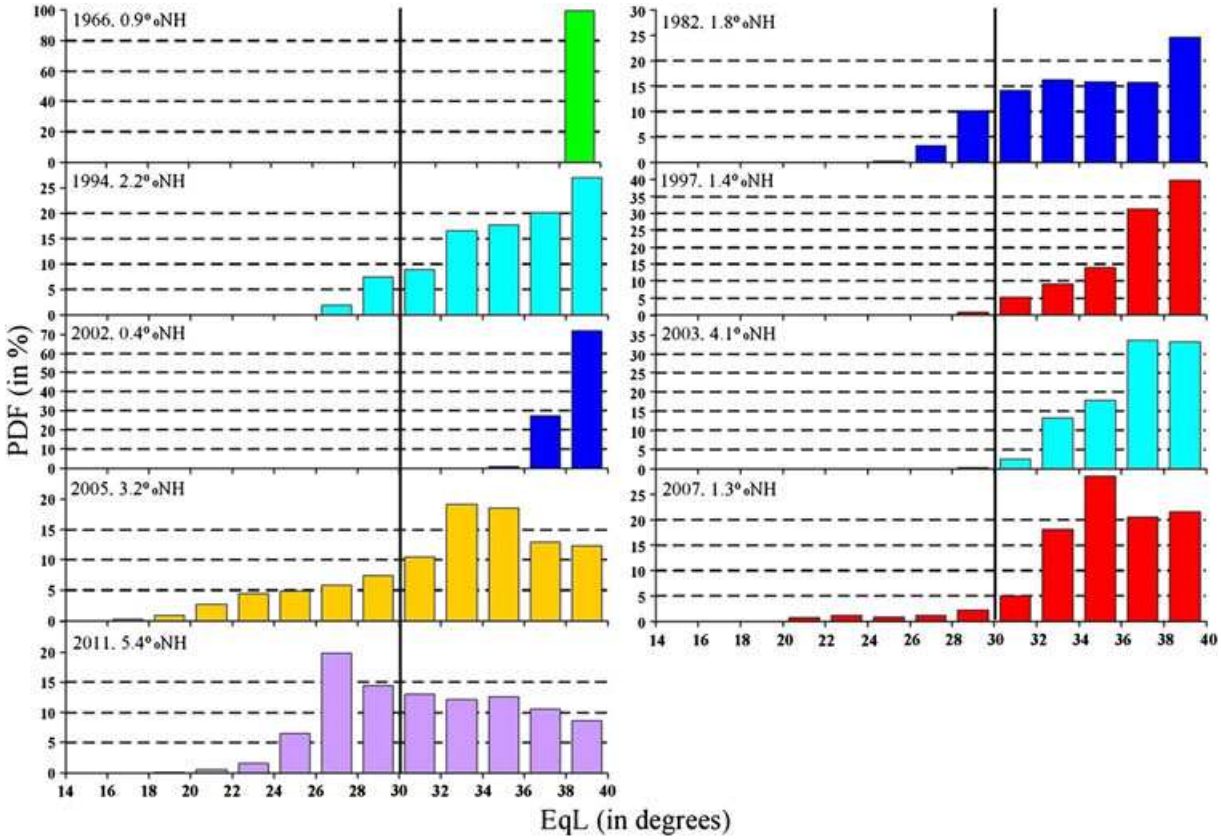

Figure 10. Probability distribution functions (PDF, in %) based on the spatial extent of the low-latitude air masses at $\Phi_{eq,lim} = 40°N$, also indicated for each histogram is %NH. Colors are chosen for different years for easy matching with Figure 5.

percentage. The spatial extent of the air masses such as $\Phi_{eq,lim}$ is lower or equal to 40°N is indicated on each histogram (in %NH). The 2003 and 2011 FrIACs events are characterized by the largest amount of low-latitude air masses into the polar region (4.1%NH and 5.4%NH, respectively). Hence, the 2011 FrIAC has been the largest recorded over the 1960–2011 period. Inversely, the 1966 and 2002 cases have the smallest spatial extents, 0.9%NH and 0.4%NH, respectively.

[37] The PDFs show that in 1966 and 2002, the air masses originate from regions located northward of 38°N and 34°N, respectively. Thus, these FrIACs contain air masses of midlatitude origin exclusively and not from a deep tropical origin. They are consequently the weakest recorded. In 1997 and 2003, the low-latitude air masses originate at the boundary between the subtropics and the midlatitudes (i.e., northward of 28°N and 30°N). The 1982, 1994, 2005, 2007, and 2011 events show an appreciable amount of air masses coming deeper in the tropics (e.g., latitudes below 30°N).

[38] These results show that the origin of the low-latitude air masses associated with FrIACs displays a high degree of interannual variability. By cumulating the PDFs for latitudes lower than 30°N, we obtain that 0.0%, 13.5%, 9.4%, 0.8%, 0.0%, 0.1%, 26.6%, 6.4%, and 43.0% of tropical/subtropical air masses in years 1966, 1982, 1994, 1997, 2002, 2003, 2005, 2007, and 2011, respectively. This shows that the 2011 FrIAC has been the strongest since 1960, supporting the findings of *Allen et al.* [2012] over a longer period.

6. Discussion

[39] These FrIAC occurrences are largely consistent with those of *Allen et al.* [2012]. Exceptions are in 2000 and 2004, when they found weak TrEL reductions at high latitudes. Although we classified these two years as Type B, these anticyclones trapped air masses from the midlatitudes rather than from the low latitudes. By examining $L_{GPH\text{-}PV}$ for both years, we also found that no bowl-shaped structure developed so that we do not classify these events as FrIACs. Furthermore, the 2007 event led to a very weak TrEL reduction at the pole in *Allen et al.* [2012], yet we do classify it clearly as a FrIAC, albeit of small spatial extent (Figure 7h or *Thiéblemont et al.*, 2011). These small discrepancies between the two studies are mostly due to the criteria used to define what a FrIAC is. It appears to us that low TrEL at the pole does not necessarily imply the occurrence of a FrIAC. In the real atmosphere, there is a whole continuum of intrusions of varying durations or spatial extents, trapping air from either low or midlatitudes, some extending north of 60°N. Hence, there is no unique way to describe these slightly different phenomena. In our case, to classify an event as a FrIAC, we require that the intrusion contains air masses from low latitudes (below $\Phi_{eq,lim} = 40°N$), reaches beyond 60°N, and is colocated with an anticyclonic

eddy. In addition, we require that this colocation of the low-PV and anticyclonic anomalies persists until the mean date of the shearing phase (May 15). The duration is not included in the criteria per se, although, as we shall see, the years with FrIACs have a persistence of intrusions beyond 20 days in all but one case (i.e., 2002).

[40] To place occurrences of FrIAC events in a climatological context, an overview of the dynamical conditions around the turnover date is shown on Figure 11. The Type-A years are marked with black dots. Type-B years without FrIAC are marked with gray dots and those with a FrIAC with a star. The dynamical conditions are characterized in terms of (a) the persistence of low-latitude intrusions into the polar region, (b) the turnover date (as in Figure 3), and (c) the eddy heat flux at the onset of the turnover, averaged in the [40,70]°N latitude band and at 30 hPa. The persistence of the low-latitude intrusions is defined as the duration beyond the turnover date, over which the spatial extent of the air masses S_{lim} falls below the 0.3%NH threshold (see also Figure 5). Note that if the low-latitude intrusion disappears before the turnover, the persistence defined above as a relative date is a negative number; for the years 1971, 1979, 1981, 1984, 1987, 1999, and 2009, the intrusions disappeared more than a month before the turnover and are not represented on the diagram.

[41] The persistence of intrusions displays a high degree of interannual variability (Figure 11a), especially during the 1980s and after 2000 when the highest amplitude variations from 1 year to the next are found. Conversely, during the mid-1970s and the 1990s, the interannual variability is quite weak, the persistence not lasting beyond 20 days. It is also anticorrelated with the time series of the turnover date (Figure 11b, left). Moreover, the eddy heat flux at the onset of the turnover (Figure 11c, left) is also correlated with the intrusion persistence (Figure 11c, right). On the scatter diagrams on Figures 11b and 11c (right), linear regression lines are drawn, and these correlations (R^2) are calculated to be -0.65 and 0.68, respectively. In other words, a long persistence of intrusions is generally associated with an early turnover date, and vice versa. Similarly, a long persistence of intrusions is generally associated with a strong heat flux pulse.

[42] We suggest that these correlations can be linked to the occurrence of intense midwinter major SSWs. Recently, the 2001 [*Jacobi et al*., 2003], 2006, 2009 [*Orsolini et al*., 2010], and 2010 [*Ayarzagüena et al*., 2011] winters were marked by intense midwinter major SSWs: with easterlies propagating well below the 10 hPa usual pressure level used to define major SSWs [*WMO*, 2007]. These intense major SSWs were followed by the recovery of a weak polar vortex and a particularly weak wave activity as revealed by Figures 6 and 7 in *Thiéblemont et al*. [2011]. We find intense major SSWs during the 1963, 1971, 1973, 1979, 1984, 1987, 1989, and 1999 winters (also reported by *Charlton and Polvani* [2007]). All these years correspond to Type A. They are characterized by an unusual weak

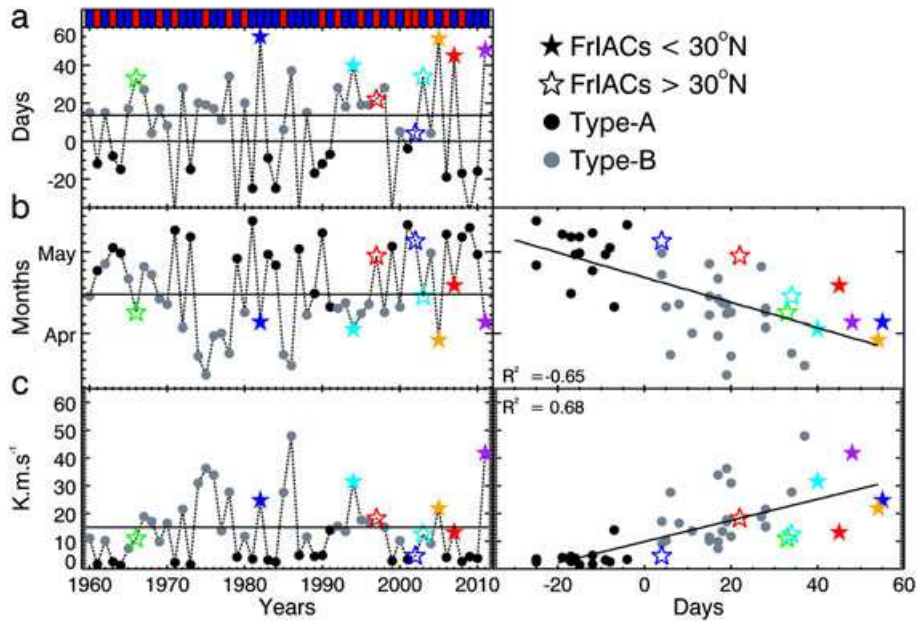

Figure 11. (a) Low-latitude intrusion persistence (in days, relative to the turnover date, see text) from 1960 to 2011. The black dots correspond to Type-A years, while non-FrIAC Type-B years are represented by gray dots. The filled (unfilled) stars correspond years where air masses inside FrIACs are with (without) a tropical/subtropical signature (see Figure 10). Colors for each star refer to those of Figure 5. (b, left) Turnover date over the same period. (c, left) Meridional eddy heat flux averaged over the [40,70]°N latitude range and from -10 to 10 days around the turnover date, at 30 hPa. Also shown are scatter plots of the turnover date (b, right) and of the heat flux (c, right) versus the persistence, as shown in (a). Horizontal black lines display the mean values over the period 1960–2011. The coefficient of correlation with respect to persistence is indicated on the two plots on the right. The easterly and westerly phases of the QBO (at 10 hPa and 0°N) on the turnover date are displayed in blue and red, respectively, on top of panel (a).

persistence of the low-latitude intrusions, a late turnover (i.e., late April/early May), and a weak eddy heat flux value (Figure 11). In other words, when such an intense major SSW occurs in midwinter and a wind reversal occurs, the upward propagation of wave activity is prohibited by the easterlies [*Tomikawa*, 2010]. While the westerlies recover due to radiative cooling, the wave activity remains weak, hindering the intrusion of low-latitude air masses to the polar region and consequently, the occurrence of FrIACs. Conversely, in the absence of these intense major SSWs, the upward wave propagation can be maintained until spring and drive the turnover, leading to strong low-latitude intrusions which are able to form FrIACs. These results are in agreement with those published by *Thiéblemont et al*. [2011] over a more extended period going back to 1960.

[43] FrIACs are overwhelmingly persistent low-latitude intrusions that tend to occur for early turnover dates and accompanied by strong heat flux pulses. In Figure 11, FrIACs displaying tropical/subtropical air masses are differentiated from the others by filled star marks. Regarding both scatter diagrams (Figure 11, right), while 1966, 1997, 2002, and 2003 cases (unfilled stars) are located in the main Type-B region, the 1982, 1994, 2005, 2007, and 2011 ones (filled star) are located on the extreme right-hand side with low-latitude intrusion persistencies higher than 40 days. We indicated the QBO phase over the 1960–2011 period on the top of Figure 11 (blue or red stripes for easterly or westerly phase, respectively). This emphasizes that FrIACs with a tropical/subtropical signature occur when the QBO is on its easterly phase. These results support previous findings of *Thiéblemont et al*. [2011] who showed that low-latitude intrusions to polar latitudes were favored under an easterly phase of the QBO, based on calculations over the period 2000–2009. Note that compared to the others, the 2002 FrIAC exposes an outlier nature associated with a very weak eddy heat flux, a late turnover and, as mentioned before, with a small spatial extent and without tropical air masses inside.

[44] Considered in a climatological context, most of FrIACs appear to be extreme events among Type-B years. FrIACs also seem to be specific features of the last decade as five events occurred since 2002. Conversely, we find that their frequency of occurrence has been extremely low prior to 2002, as only four events are identified over 42 years (1960–2001). In this study, we cannot fully explain why such extreme events did not appear more often before, while the number of Type-B years remains approximately constant for each decade (between 5 and 7 Type-B years per decade). As we show with the example in 1986 (see section 5.2), we observe an in-phase relationship between the low-latitude intrusion and the anticyclone, but the eddy heat flux time series reveals secondary pulses which contribute to dissociating the intrusion from the anticyclonic anomaly. Such a mechanism preventing FrIACs occcurrences has also been identified in some other Type-B years in the 1990s (not shown). These latter results suggest that FrIAC occurrences are highly sensitive to the complexities of stratospheric dynamical variability. In the 1970s, no "bowls" characterizing FrIACs are diagnosed despite the sizeable long-lived intrusions, the early turnovers, the large pulse of eddy heat flux at the onset of the turnover and the absence of secondary heat flux pulses. After examining qualitatively all the MIMOSA PV maps and the associated eddy geopotential height anomalies for these years, we did not find evidence of FrIACs. The particularly low FrIAC frequency of occurrences from 1960 to 1980 is puzzling. We surmise that the absence of satellite measurements in the assimilation systems during this period is probably an important factor for the quality of stratospheric analyses in general and for the tropical to polar stratospheric transport in particular. Low FrIAC occurrences in the presatellite era could be due to a poor representation of winds and wind shears in the critical subtropical region or of high-latitude coherent eddies.

7. Conclusion

[45] The 2010–2011 winter was characterized by an unusually cold and undisturbed polar vortex which led to the highest ozone depletion ever recorded [*Manney et al*., 2011]. The 2011 spring was also characterized by the occurrence of an exceptionally large FrIAC event, whereby, at the onset of the transition to the easterly regime, a large intrusion of warm, low-latitude air was pulled toward the polar region and remained there, confined within a strong anticyclone, for several weeks. The evolution of this intrusion into a FrIAC event is nicely captured by the PV advection model MIMOSA. As the QBO was in its easterly phase and no intense major stratospheric warming occurred during midwinter in 2011, the dynamical conditions were identified as propitious to the development of a FrIAC [*Thiéblemont et al*., 2011].

[46] The exceptional characteristics of this new event, i.e., the spatial extent and the tropical origin of the air masses within the FrIAC, motivated us to establish a detailed climatology of FrIACs over the period 1960–2011. To cover the whole period, it was necessary to use both ERA-40 and ERA-Interim reanalyses, as the latter only start in 1979. Analyzed fields have been used to initialize and force the MIMOSA PV advection model from January to June each year. To detect low-latitude intrusions in the spring polar stratosphere and to quantify their characteristics (spatial extent, duration), we developed a method based on the equivalent latitude diagnostic calculated from the advected PV of the MIMOSA model. While strong, lasting intrusions are observed in many years (33 of 52), not all developed into FrIAC events, which correspond to a characteristic trapping of low-latitude air masses within a relatively long-lived anticyclone. To confirm the FrIAC occurrences, we calculated the distance between geopotential height positive anomalies and the low-PV in the intrusion and determined when they were in-phase. We thus were able to detect 9 FrIACs events: in 1966, 1982, 1994, 1997, 2002, 2003, 2005, 2007, and 2011.

[47] We also studied the latitudinal origin of the air masses captured in the FrIACs. The results show that the 2011 event was not only the largest in spatial extent but also contained the largest amount of tropical air (meaning air originating equatorwards of 30°N), again in agreement with the results of *Allen et al*. [2012]. Conversely, the 1966 and 2002 events have been the weakest, predominantly capturing midlatitude air masses. Our climatology shows that FrIACs occurred overall in association with abrupt and early reversal to summer easterlies and a large heat flux pulse around the date of this wind reversal. These conditions are identified to be

favored in the absence of intense midwinter major warming. Furthermore, FrIACs containing air masses originating closer to the equator (1982, 1994, 2005, 2007, and 2011) are favored when the QBO displays an easterly phase. These results are in agreement with findings of *Thiéblemont et al*. [2011]. The two favorable conditions are not necessarily fully prognostic, however. We also show that, in some cases, a prolonged heat flux pulse a few days after the turnover can displace potential FrIAC events from the polar region to midlatitudes, where their signature dissipates. This suggests that FrIAC occurrences highly depend on the complexities of stratospheric dynamical variability.

[48] FrIACs appear to be extreme low-latitude air masse intrusion events during spring in the polar region. The most surprising results concern the FrIACs occurrence frequency. We surmise that the absence of satellite measurements in the assimilation systems during the 1960–1980 period, displaying only one FrIAC event (i.e., 1966), could be an important factor, affecting the quality of the middle stratosphere reanalyses, and thus the representation of FrIACs. Conversely, our climatology reveals that the period 2002–2011 has been marked by an exceptional number of FrIAC occurrences. While we recognize that (i) FrIACs are relatively rare events, and hence the above-mentioned decadal and interannual variability in frequency of occurrences have low significance in a trend estimation context, and that (ii) reanalyses are not entirely appropriate to examine trend issues, it appears to us that such decadal variability in the coupling of low and high latitudes in the Northern Hemisphere spring stratosphere deserves further investigation.

[49] **Acknowledgments.** This study has been conducted within the framework of the STRAPOLETE project supported by the "Agence Nationale de la Recherche ANR (STRAPOLETE project ANR 08 BLAN 0300), the "Institut Polaire Paul Emile Victor" (IPEV), and the "Centre National d'Etudes Spatiales (CNES)". YOR was partially funded by the EC-FP7 project RECONCILE (Grant number: RECONCILE-226365-FP7-ENV-2008-1). We thank ETHER for access to database (Pôle thématique du CNES) and the European Centre for Medium-Range Weather Forecasts for providing the ERA-40 and ERA-Interim data. We thank Johanna Gonçalves for helping us with ERA data and Tjarda Roberts for helping us with English grammar. Finally, we thank the five anonymous referees for their helpful comments and suggestions to improve this work.

References

Andrews, D. G., J. R. Holton, and C. B. Leovy (1987), in *Middle Atmosphere Dynamics*, 489 pp., Academic, San Diego, Calif.

Allen, D. R., and N. Nakamura (2003), Tracer equivalent latitude: a diagnostic tool for isentropic transport studies, *J. Atmos. Sci.*, *60*, 287–304.

Allen, D. R., A. R. Douglass, G. L. Manney, S. E. Strahan, J. C. Krosschell, J. V. Trueblood, J. E. Nielsen, S. Pawson, and Z. Zhu (2011), Modeling the Frozen-In Anticyclone in the 2005 Arctic Summer Stratosphere, *Atmos. Chem. Phys.*, *11*, 4557–4576, doi:10.5194/acp-11-4557-2011.

Allen, D. R., A. R. Douglass, G. E. Nedoluha, and L. Coy (2012), Tracer transport during the Arctic stratospheric final warming based on a 33-year (1979-2011) tracer equivalent latitude simulation, *Geophys. Res. Lett.*, *39*, L12801, doi:10.1029/2012GL051930.

Ayarzagüena, B., and E. Serrano (2009), Monthly characterization of the tropospheric circulation over the Euro-Atlantic area in relation with the timing of stratospheric final warming, *J. Climate*, *22*, 6313–6324.

Ayarzagüena, B., U. Langematz, and E. Serrano (2011), Tropospheric forcing of the stratosphere: A comparative study of the two different major stratospheric warmings in 2009 and 2010, *J. Geophys. Res.*, *116*, D18114, doi:10.1029/2010JD015023.

Black, R. X., B. A. McDaniel, and W. A. Robinson (2006), Stratosphere-Troposphere coupling during spring onset, *J. Climate*, *19*, 4891–4901.

Black, R. X., and B. A. McDaniel (2007), The dynamics of Northern Hemisphere stratospheric final warming events, *J. Atmos. Sci.*, *64*, 2932–2946.

Charlton, A. J., and Polvani, L. M. (2007), A new look at stratospheric sudden warmings. Part I. Climatology and modeling benchmarks, *J. Climate*, *20*, 449–471, doi:10.1175/JCLI3996.1.

Dee, D. P., et al. (2011), The ERA-Interim reanalyses: configuration and performance of the data assimilation system, *Q. J. R. Meteorol. Soc.*, *137*, 553–597, doi:10.1002/qj.828

Durry, G., and A. Hauchecorne (2005), Evidence for long-lived polar vortex air in the mid-latitudes summer stratosphere from in situ laser diode CH_4 and H_2O measurements, *Atmos. Chem. Phys.*, *5*, 1467–1472.

Godin, S., M. Marchand, A. Hauchecorne, and F. Lefèvre (2002), Influence of Arctic polar ozone depletion on lower stratospheric ozone amounts at Haute-Provence Observatory (43.92°N, 5.71°E), *J. Geophys. Res.*, *107*, 8272, doi:10.1029/2001JD000516.

Harvey, V. L., and M. H. Hitchman (1996), A Climatology of the Aleutian High, *J. Atmos. Sci.*, *53*, 2088–2100.

Harvey, V. L., R. B. Pierce, T. D. Fairlie, and M. H. Hitchman (2002), A climatology of stratospheric polar vortices and anticyclones, *J. Geophys. Res.*, *107*, 4442, doi:10.1029/2001JD001471.

Hauchecorne, A., S. Godin, M. Marchand, B. Heese, and C. Souprayen (2002), Quantification of the transport of chemical constituents from the polar vortex to midlatitudes in the lower stratosphere using the high-resolution advection model MIMOSA and effective diffusivity, *J. Geophys. Res.*, Vol. *107*, No. D20, 8289, doi:10.1029/2001JD000491.

Hess, P. G. (1991), Mixing processes following the final stratospheric warming, *J. Atmos. Sci*, *48*, 1625–1641.

Huret, N., M. Pirre, A. Hauchecorne, C. Robert, and V. Catoire (2006), On the vertical structure of the stratosphere at midlatitudes during the first stage of the polar vortex formation and in the polar region in the presence of a large mesospheric descent, *J. Geophys. Res.*, *111*(D06111), doi:10.1029/2005JD006102.

Hurwitz, M. M., P. A. Newman, and C. I. Garfinkel (2011), The Arctic vortex in March 2011: A dynamical perspective, *Atmos. Chem. Phys.*, *11*, 11,447–11,453.

Jacobi, C., D. Kürschner, H. G. Muller, D. Pancheva, N. J. Mitchell, and B. Naujokat (2003), Response of the mesopause region dynamics to the February 2001 stratospheric warming, *J. Atmos. Sol.-Terr. Phys.*, *65*, 843–855.

Lahoz, W. A., A. J. Geer, and Y. J. Orsolini (2007), Northern Hemisphere stratospheric summer from MIPAS observations, *Q. J. R. Meteorol. Soc.*, *133*, 197–211.

Lait, L. R. (1994), An Alternative Form for Potential Vorticity, *J. Atmos. Sci.*, *51*, 1754–1759.

Leblanc, T., I. S. McDermid, and A. Hauchecorne (2004), A study of ozone variability and its connection with meridional transport in the northern Pacific lower stratosphere during summer 2002, *J. Geophys. Res.*, *109*, D11105, doi:10.1029/2003JD004027.

Manney, G. L., N. J. Livesey, C. J. Jimenez, H. C. Pumphrey, M. L. Santee, I. A. MacKenzie, and J. W. Waters (2006), EOS Microwave Limb Sounder observations of "frozen-in" anticyclonic air in Arctic summer, *Geo. Res. Let.*, Vol. *33*, L06810, doi:10.1029/2005GL025418.

Manney, G., et al. (2011), Unprecedented Arctic ozone loss in 2011, *Nature*, *478*, 469–475.

Marchand, M., S. Godin, A. Hauchecorne, F. Lefèvre, S. Bekki, and M. Chipperfield (2003), Influence of polar ozone loss on northern midlatitude regions estimated by a high-resolution chemistry transport model during winter 1999/2000, *J. Geophys. Res.*, *108*, 8326, doi:10.1029/2001JD000906.

Matthewman, N. J., J. G. Esler, A. J. Charlton-Perez, and L. M. Polvani (2009), A new look at stratospheric sudden warmings. Part III: Polar vortex evolution and vertical structure, *J. Clim.*, *22*, 1566–1585.

Nishii, K., H. Nakamura, and Y. J. Orsolini (2011), Regional Geographical dependence of blocking high contributions to the stratospheric variability through enhancement and suppression of upward planetary-wave propagation, *J. Climate*, *24*, 6408–6423. doi:10.1175/JCLI-D-10-05021.

Orsolini, Y. J. (2001), Long-lived tracer patterns in the summer polar stratosphere, *Geo. Res. Let.*, Vol. *28*, No. 20, 3855–3858.

Orsolini, Y. J., J. Urban, D. P. Murtagh, S. Lossow, and V. Limpasuvan (2010), Descent from the polar mesosphere and anomalously high stratopause observed in 8 years of water vapor and temperature satellite observations by the Odin Sub-Millimeter Radiometer, *J. Geophys. Res.*, *115*, D12305, doi:10.1029/2009JD013501.

Thiéblemont, R., N. Huret, Y. J. Orsolini, A. Hauchecorne, and M.-A. Drouin (2011), Frozen-in anticyclones occurring in polar Northern Hemisphere during springtime: Characterization, occurrence and link with quasi-biennial oscillation, *J. Geophys. Res.*, *116*, D20110, doi:10.1029/2011JD016042.

Tomikawa, Y. (2010), Persistence of Easterly Wind during Major Stratospheric Sudden Warmings, *J. Climate*, *23*, 5258–5267, doi:10.1175/2010JCLI3507.1.

Uppala, S. M., et al. (2005), The ERA-40 re-analysis, *Q. J. R. Meteorol. Soc.*, *131*, 2961–3012, doi:10.1256/qj.04.176.

Waugh, D. W., and P. P. Rong (2002), Interannual variability in the decay of lower stratospheric Arctic vortices, *J. Meteorol. Soc. Jpn.*, *80*, 997–1012.

Waugh, D. W. and L. M. Polvani (2010), Stratospheric Polar Vortices, in '*The Stratosphere: Dynamics, Transport and Chemistry*'. A festschrift celebrating Alan Pumb's 60th birthday, L. M. Polvani, A. H. Sobel and D. W. Waugh, Eds., American Geophysical Union, Washington, D.C.

WMO (World Meteorological Organization), Scientific Assessment of Ozone Depletion: 2006, Global Ozone Research and Monitoring Project-Report No. 50, 572 pp., Geneva, Switzerland, 2007.